monopoles from antimonopoles, which are requirements in other types of searches.[5,6])

The detector we have described is unusually free of background in the presence of both highly radioactive sources and cosmic-ray background, having detected only one count in a 10-day running period.

*Work supported in part by the U. S. Atomic Energy Commission.

[1]Such a phenomenon might in fact account for the non-observation of magnetic monopoles. If magnetic monopoles were too massive to be produced at accelerator energies they could still be produced at cosmic-ray energies in undisturbed moon rocks. Over the long life of the moon appreciable numbers of monopoles could have been produced even in the small cosmic-ray fluxes. If, however, the magnetic monopole decayed, violating monopole charge conservation, one could not predict its lifetime. However, the probability of observing magnetic monopoles in moon rocks would then be reduced by the ratio of the decay lifetime of the monopole to the age of the moon. This might be an exceedingly small number.

[2]B. Pontecorvo, Yad. Fiz. 11, 846 (1970) [Sov. J. Nucl. Phys. 11, 473 (1970)].

[3]A. V. Dem'Yanov, A. V. Kulikov, A. B. Kuptsov, G. G. Mkrtchyan, L. L. Nemenov, B. M. Pontecorvo, G. I. Smirnov, D. M. Khazins, and Yu M. Chirkin, Yad. Fiz. 13, 786 (1971) [Sov. J. Nucl. Phys. 13, 447 (1971)].

[4]T. J. Droege, Princeton-Pennsylvania Accelerator Report No. PPAD-605E, 1966 (unpublished).

[5]R. A. Carrigan and F. A. Nezrick, Phys. Rev. D 3, 56 (1971).

[6]P. H. Eberhard, R. R. Ross, L. W. Alvarez, and R. D. Watt, Phys. Rev. D 4, 3260 (1971).

PHYSICAL REVIEW D VOLUME 9, NUMBER 7 1 APRIL 1974

$K_L^0 p \to K_S^0 p$ scattering from 1 to 10 GeV/c*

G. W. Brandenburg, W. B. Johnson, D. W. G. S. Leith, J. S. Loos,† G. J. Luste,‡ J. A. J. Matthews, K. Moriyasu,§ W. M. Smart,|| F. C. Winkelmann,** and R. J. Yamartino††

Stanford Linear Accelerator Center, Stanford University, Stanford, California 94305

(Received 5 November 1973)

The differential cross sections for $K_L^0 p \to K_S^0 p$ scattering are presented in several momentum intervals between 1 and 10 GeV/c. The data are strongly peaked in the forward direction, characteristic of a large s-channel helicity-nonflip scattering amplitude in this reaction, and a distinct break in the differential cross section occurs at $|t| = 0.3$ GeV^2. The phase of the forward scattering amplitude, ϕ, is consistent with being independent of momentum. The average value of the phase, $\phi = -133.9 \pm 4.0°$, corresponds to a Regge trajectory $\alpha(0) = 0.49 \pm 0.05$ in agreement with the canonical ρ, ω^0 Regge intercept, $\alpha(0) \sim 0.5$. However, this result disagrees with the Regge trajectory determined from the energy dependence of the forward cross section, $\alpha(0) = 0.30 \pm 0.03$, indicating a breaking of the Regge phase-energy relation. Comparisons of $K_L^0 p \to K_S^0 p$ and $\pi^- p \to \pi^0 n$ scattering data reveal substantial differences in the energy dependence of the differential cross sections. Comparisons to KN charge-exchange data then suggest that direct-channel (absorption) effects may explain the differences in πN and KN channels.

I. INTRODUCTION

The simple structure of $K_L^0 p \to K_S^0 p$ scattering makes this a particularly relevant reaction in the study of two-body interactions. Of the known hyperons only Σ resonances can be formed in the low-energy or s-channel scattering region. Similarly, in the u channel the reaction $K^0 p \to pK^0$ allows only Σ exchange, whereas the channel $\bar{K}^0 p \to p\bar{K}^0$ is exotic. In the t channel, only mesons with natural spin-parity and odd charge conjugation can be exchanged; of the possible candidates, ρ and ω contributions are thought to dominate. Thus, the reaction $K_L^0 p \to K_S^0 p$ can be considered the Kp scattering analog of $\pi^- p \to \pi^0 n$ scattering. This similarity will be exploited in our analysis.

Previous results on the reaction $K_L^0 p \to K_S^0 p$ have come primarily from K_S^0 coherent regeneration experiments[1-3]; however, these analyses determine the scattering amplitude only at $t = 0$. In contrast, the present experimental results provide complete angular distributions for $K_L^0 p \to K_S^0 p$ scattering in the momentum interval 1 to 10 GeV/c.[4]

Details of the experiment are described in Sec. II. Qualitative features of the data and the differential and total cross sections for $K_L^0 p \to K_S^0 p$ scattering are discussed in Sec. III. The forward $K_L^0 p \to K_S^0 p$ differential cross sections are then discussed in detail in Sec. IV. Finally, in Sec. V the tabular results and a brief summary of our large-angle analyses[5] are presented. Section VI contains the summary and conclusions.

II. EXPERIMENTAL DETAILS

The $K_L^0 p \to K_S^0 p$ data come from an approximately one-million-picture exposure of the SLAC 40-in. hydrogen bubble chamber to a K_L^0 beam. The typical K_L^0 flux was between 20 and 40 K_L^0/pulse over the momentum interval ~600 MeV/c to ~12 GeV/c. The beam spectrum peaked at ~4 GeV/c, decreasing to < 10% of maximum intensity at momenta of ~1 and 11 GeV/c. Details on the construction of the beam and the K_L^0 momentum spectrum are discussed elsewhere.[6]

The film was scanned once with approximately 10% of the film rescanned a second time. In addition, a special scan for backward-vee events (events with the laboratory scattering angle of the K_S^0, $\theta_{lab} > 45°$) was made on ~15% of the film. Scan efficiencies, as well as corrections for losses of events with steeply dipping (primarily short) protons were determined as a function of momentum transfer. These two corrections were consistent with being uncorrelated and with being independent of beam momentum. The scan efficiencies and azimuthal loss corrections are recorded in Table I for events with momentum transfers $|t| > 0.025$ GeV^2. For events with $|t| < 0.025$ GeV^2 (proton ranges in the bubble chamber $\lesssim 1.5$ cm) the statistics were too sparse to determine the scanning efficiencies; therefore the data in this interval have been omitted.

TABLE I. Scanning efficiencies determined for $K_L^0 p \to K_S^0 p$.

Momentum transfer interval $\lvert\Delta t\rvert$ (GeV^2)	Scan efficiency (%)	Azimuthal loss correction
0.025–0.05	50 ± 20	1.30 ± 0.08
0.05–0.1	80 ± 12	1.14 ± 0.05
0.1–0.2	90 ± 7	1.10 ± 0.04
0.2–0.4	94 ± 4	
>0.4 and $\theta_{lab} \leq 45°$ [a]		1.05 ± 0.02
$\theta_{lab} > 45°$	74 ± 10	

[a] θ_{lab} is the laboratory scattering angle of the K_S^0. For initial K_L^0 momenta $\gtrsim 1$ GeV/c, a laboratory scattering angle $\theta_{lab} \geq 45°$ corresponds to $\cos\theta_{c.m.} \leq 0.0$.

The fiducial regions chosen for the primary vertex and the K_S^0 decay vertex allowed at least 15 cm for the K_S^0 decay region, and at least 20 cm for measurement of the two pions from the K_S^0 decay. With this interaction region, scanning efficiencies were found to be independent of the K_S^0 decay lengths, $l_{K_S^0}$ for $0.3 \leq l_{K_S^0} \leq 20$ cm. For K_S^0 decay lengths $l_{K_S^0} > 20$ cm corrections were

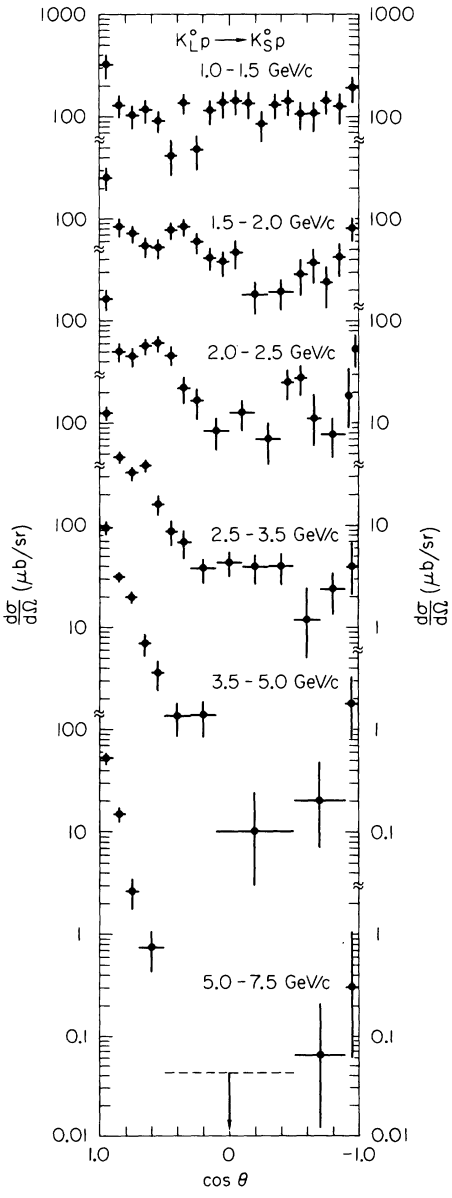

FIG. 1. Differential cross sections for $K_L^0 p \to K_S^0 p$ in six momentum intervals between 1.0 and 7.5 GeV/c. The dashed error bar in the highest momentum data indicates the 85% confidence level upper limit on this cross section (this corresponds to 1.9 events when no events are observed).

TABLE II. Differential cross sections: $(d\sigma/d\Omega)(K_L^0 p \to K_S^0 p)$.

$\cos\theta$ interval \ P_{lab} (GeV/c)	1.0–1.5	1.5–2.0	2.0–2.5	2.5–3.5	3.5–5.0	5.0–7.5
			$(d\sigma/d\Omega)$ (μb/sr)			
1.0–0.9	319 ±87.5	246 ±59.6	167 ±34.2	125 ±19.7	95.3±14.7	52.8 ±8.3
0.9–0.8	128 ±31.7	83.6±17.4	49.8±10.3	47.1±6.18	30.7±3.8	15.3 ±2.5
0.8–0.7	103 ±27.4	69.4±14.5	44.5±9.0	32.0±4.82	19.9±2.9	2.57±0.87
0.7–0.6	111 ±27.3	53.6±12.4	57.2±10.3	37.7±5.22	6.9±1.7	0.73±0.30
0.6–0.5	89.8±23.1	52.1±11.9	60.7±10.8	15.7±3.30	3.6±1.1	
0.5–0.4	40.0±14.3	77.2±15.1	44.5±9.2	8.6±2.3	1.3±0.5	<0.043
0.4–0.3	137 ±30.9	83.0±15.5	21.2±6.2	6.7±2.0		
0.3–0.2	48.4±17.3	60.0±13.1	16.2±5.7	3.7±1.0	1.3±0.5	
0.2–0.1	115 ±30.8	41.5±10.6	8.0±2.7			
0.1–0.0	137 ±40.1	36.0±9.9		4.2±1.1		
0.0–−0.1	141 ±38.5	46.9±14.0	12.0±3.9			
−0.1–−0.2	138 ±38.6	17.8±6.1		3.9±1.3	$0.10^{+0.14}_{-0.08}$	
−0.2–−0.3	85.1±28.2		6.6±2.9			
−0.3–−0.4	128 ±36.7	19.0±6.3		4.0±1.4		
−0.4–−0.5	138 ±37.7		23.7±7.9			
−0.5–−0.6	106 ±31.9	28.4±10.8	26.2±8.4	$1.2^{+1.2}_{-0.7}$		$0.064^{+0.156}_{-0.052}$
−0.6–−0.7	107 ±33.2	36.7±13.3	$10.7^{+7.9}_{-4.9}$		$0.20^{+0.27}_{-0.13}$	
−0.7–−0.8	142 ±37.5	23.8±10.2	7.9±3.2	2.4±1.0		
−0.8–−0.9	124 ±37.4	41.4±14.3				
−0.9–−0.95	188 ±50.5	81.1±21.3	$18.4^{+15.7}_{-9.5}$	$3.9^{+2.9}_{-1.8}$	$1.8^{+1.5}_{-0.9}$	$0.30^{+0.72}_{-0.24}$
−0.95–−1.0			53.6±18.5			

made for a slow decrease in the scanning efficiency up to $l_{K_S^0}=40$ cm, the K_S^0 decay length cutoff used in the analysis. Accepted events were weighted by the reciprocal of the detection probability:

$$W^{-1}=\exp(-l_{\min}/\lambda)-\exp(-l_{\max}/\lambda),$$

where $l_{\min}$ is 0.3 cm, $l_{\max}$ is the potential decay length to the boundary of the decay volume ($l_{\max} \leq 40$ cm), and λ is the mean decay length for a K_S^0 of the given momentum.

The events were measured both on conventional film plane machines and on the SLAC Spiral Reader, and processed with the computer programs TVGP-SQUAW . Events were accepted with kinematic reconstruction probabilities $\geq 1\%$. Contamination from the reactions $\bar{K}^0 p \to \pi^+ \Lambda^0$, $\bar{K}^0 p \to \pi^+ \Sigma^0$, $K_L^0 p \to K_L^0 p$, and $K_S^0 p \to K_S^0 p$ was determined to be $< 1\%$. The inclusion of $K_L^0 p \to K_S^0 \pi^+ n$ or $K_L^0 p \to K_S^0 \pi^0 p$ final states into the $K_L^0 p \to K_S^0 p$ data was estimated to be $\lesssim 1\%$ for forward scattering events, and $\lesssim 5\%$ for events in the backward direction, $\cos\theta_{c.m.} < -0.5$.

The final sample of $K_L^0 p \to K_S^0 p$ data used in the analysis consisted of 1929 events in the momentum interval 1 to 10 GeV/c.

III. DIFFERENTIAL AND TOTAL CROSS SECTIONS

The differential cross sections for our $K_L^0 p \to K_S^0 p$ data are shown in Fig. 1 and recorded in Table II for six momentum intervals between 1 and 7.5 GeV/c. The cross sections are corrected[7] for the unseen decay mode $K_S^0 \to \pi^0\pi^0$. The uncertainties in the data include the statistical errors as well as the uncertainties in the shape of the K_L^0 momentum spectrum, the scanning efficiency, and the azimuthal loss correction (see Sec. II). An over-all normalization uncertainty of ~ 10% has not been included, however.

To compensate for the loss of events with momentum transfers $|t| < 0.025$ GeV^2 (see Sec. II), data in the interval $0.025 \leq |t| \leq 0.25$ GeV^2 were parameterized with the form[8]

$$\frac{d\sigma}{dt}(s,t)=\left(\frac{As^m}{p_{lab}^{\ 2}}\right)\exp[(b_0+2b'\ln s)t] \qquad (1)$$

between 1 and 10 GeV/c. The $K_L^0 p \to K_S^0 p$ cross section in the interval $0.0 \leq |t| \leq 0.025$ GeV^2 was then determined from this parameterization, and included in the quoted differential cross sections for $\cos\theta > 0.9$ (see Table II) and in the $K_L^0 p \to K_S^0 p$ total cross sections.

The $K_L^0 p \to K_S^0 p$ differential cross sections are characterized by distinct peaks in the forward and backward regions (t- and u-channel Regge regions) that are observed at all energies. Some structure occurs through the entire angular distribution in the s-channel resonance region, but disappears above 3.5 GeV/c. The cross sections at backward and middle angles decrease with

energy much more rapidly than in the forward direction.

The general energy dependence of the data can be seen in Fig. 2, where the cross section for $K_L^0 p \to K_S^0 p$ is plotted as a function of beam momentum. Cross sections from previous measurements[9-11] are also included in this figure. Numerical values for the present data are recorded in Table III. For momenta above ~1 GeV/c the $K_L^0 p \to K_S^0 p$ cross sections can be parameterized with the power-law form

$$\sigma_{K_L^0 p \to K_S^0 p} = A p_{\text{lab}}^{\ -n}, \qquad (2)$$

giving $n \sim 2.1$ as shown in Table IV. This energy dependence is substantially greater than for the π induced reactions $\pi^- p \to \pi^0 n$ and $\pi^- p \to \eta^0 n$, where $n = 1.09 \pm 0.03$[12] and $n = 1.37 \pm 0.04$,[13] for data in the interval ~5 to 50 GeV/c. Somewhat better agreement is obtained from comparisons with the K induced reactions $K^- p \to \bar{K}^0 n$ and $K^+ n \to K^0 p$, where $n = 1.5 \pm 0.1$[14] and $n = 2.10 \pm 0.05$,[15] respectively.

Little structure is apparent in the $K_L^0 p \to K_S^0 p$ cross section in Fig. 2, where the data are plotted with a logarithmic scale. The low-energy data do reveal resonance enhancements, however, as shown in Fig. 3, where the cross section is replotted as a function of center-of-mass energy. These data are also recorded in Table V. Although the $K^0 p \to K^0 p$ and $\bar{K}^0 p \to \bar{K}^0 p$ channels are mixed in the data, if the exotic $K^0 p \to K^0 p$ cross section is smoothly varying with energy only Σ resonances should appear in the $K_L^0 p \to K_S^0 p$ cross section. The enhancements can in fact be explained by the known resonances, the $\Sigma(1765)$, $\Sigma(2030)$, and $\Sigma(2250)$ as indicated in Fig. 3.

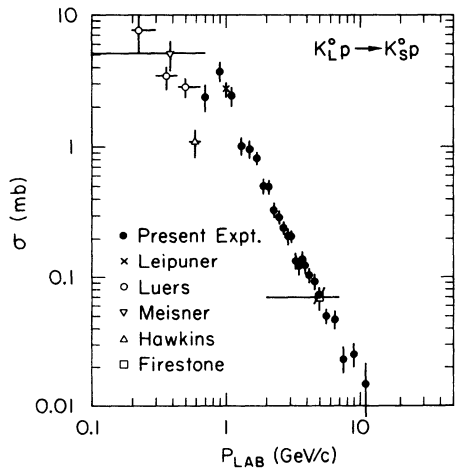

FIG. 2. Total cross section for the reaction $K_L^0 p \to K_S^0 p$. The solid points come from the present experiment; data from Refs. 9–11 are also included.

TABLE III. Total cross section for $K_L^0 p \to K_S^0 p$.

P_{lab} (GeV/c)	Events [a]	σ (μb)
0.6–0.8	44	2385 ±561
0.8–1.0	138	3692 ±633
1.0–1.2	151	2398 ±298
1.2–1.4	101	1002 ±128
1.4–1.6	132	952 ±117
1.6–1.8	153	807 ±88.5
1.8–2.0	116	501 ±61.3
2.0–2.2	130	491 ±44.2
2.2–2.4	104	329 ±32.2
2.4–2.6	104	290 ±28.1
2.6–2.8	91	241 ±24.8
2.8–3.0	84	210 ±23.5
3.0–3.2	96	205 ±20.4
3.2–3.4	58	133 ±17.5
3.4–3.6	51	120 ±17.0
3.6–3.8	66	141 ±17.3
3.8–4.0	56	123 ±16.6
4.0–4.4	87	101 ±11.0
4.4–4.8	76	90.8 ±10.4
4.8–5.2	53	73.0 ±9.9
5.2–6.0	65	49.0 ±5.8
6.0–7.0	55	47.0 ±6.4
7.0–8.0	19	23.2 ±5.2
8.0–10.0	22	25.2 ±5.1
10.0–12.0	4	$14.6^{+10.9}_{-6.6}$

[a] Totals for events with K_S^0 decay lengths $0.3 \leq l_{K_S^0} \leq 40$ cm; see Sec. II.

IV. FORWARD CROSS SECTIONS

A. Phenomenology

For $K_L^0 p \to K_S^0 p$ scattering the known t-channel exchanges are the ρ, ω^0, and ϕ mesons. Neglecting the ϕ contribution, since the $\phi N \bar{N}$ coupling is thought to be small,[16] the $K_L^0 p \to K_S^0 p$ reaction can be parameterized in terms of ρ and ω^0 exchanges.[17]

The reactions $K_L^0 p \to K_S^0 p$ and $\pi^- p \to \pi^0 n$ can then be related by adopting a particular model for the coupling constants. For example, assuming SU(3) we obtain

$$A_{\pi^- p \to \pi^0 n} = -\sqrt{2}\,\rho \equiv -\sqrt{2}\,V$$

and (3)

$$A_{K_L^0 p \to K_S^0 p} = -\tfrac{1}{2}[(4F-1)\omega^0 - \rho] \equiv -(2F-1)V,$$

where the exchange degeneracy of ρ and ω^0 Regge trajectories is used to equate these amplitudes to a "universal" vector exchange amplitude $V(s, t)$. In Eq. (3) the symmetric and antisymmetric SU(3) octet couplings are defined such that $F + D = 1$. Similar relations also follow for the differences

TABLE IV. Energy dependence of the $K_L^0 p \to K_S^0 p$ cross section, $\sigma_{K_L^0 p \to K_S^0 p} = Ap^{-n}$.

Momentum interval (GeV/c)	A (μb)	n
1.0–12.0	2255 ± 114	2.18 ± 0.05
2.5–12.0	1812 ± 241	2.02 ± 0.10
4.0–12.0	2000 ± 767	2.07 ± 0.23

of πN and KN total cross sections. These can be obtained from the optical-theorem results:

$$\Delta\sigma_{\pi^\pm p}^{\text{tot}} = \sigma_{\pi^- p}^{\text{tot}} - \sigma_{\pi^+ p}^{\text{tot}} \equiv -\frac{4\sqrt{2}\,\pi}{k}\,\text{Im}A_{\pi^- p \to \pi^0 n} \quad (4a)$$

and

$$\Delta\sigma_{K^\pm n}^{\text{tot}} = \sigma_{K^- n}^{\text{tot}} - \sigma_{K^+ n}^{\text{tot}} \equiv -\frac{8\pi}{k}\,\text{Im}A_{K_L^0 p \to K_S^0 p}\,. \quad (4b)$$

For the present analysis the scattering will be discussed in terms of s-channel helicity amplitudes, $f_{\Delta\lambda}$, where the net helicity flip in the reaction is specified by $\Delta\lambda$. From hypercharge-exchange reactions estimates of the SU(3) factor F [see Eq. (3)] have been obtained for both helicity-flip and helicity-nonflip amplitudes[18]:

$$F_{\Delta\lambda=0} \sim 1.25$$

and (5)

$$F_{\Delta\lambda=1} \sim 0.25\,.$$

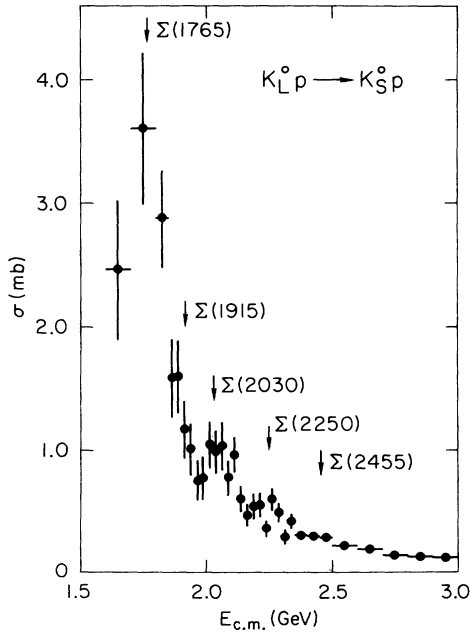

FIG. 3. Cross section for the reaction $K_L^0 p \to K_S^0 p$ in the resonance region. The masses of known Σ resonances are included for comparison with the data.

Using these values, we observe [cf. Eq. (3)] that the ω^0 contribution should dominate the ρ contribution to the $K_L^0 p \to K_S^0 p$ helicity-nonflip amplitude. However, the ω^0 approximately decouples from the helicity-flip amplitude such that

$$f_{\Delta\lambda=1}(K_L^0 p \to K_S^0 p) \approx -\tfrac{1}{2}\rho = \frac{-1}{2\sqrt{2}} f_{\Delta\lambda=1}(\pi^- p \to \pi^0 n)\,. \quad (6)$$

This yields an estimate for the helicity-flip contribution to the $K_L^0 p \to K_S^0 p$ cross section:

$$\left(\frac{d\sigma}{dt}\right)_{\Delta\lambda=1}(K_L^0 p \to K_S^0 p) \approx \frac{1}{8}\left(\frac{d\sigma}{dt}\right)(\pi^- p \to \pi^0 n), \quad (7)$$

where the $\pi^- p \to \pi^0 n$ cross section is taken to be dominantly helicity-flip.[19–21]

B. Differential cross sections

The forward differential cross sections for our data are shown in Fig. 4 and recorded in Table VI

TABLE V. Cross section for $K_L^0 p \to K_S^0 p$ in the resonance region.

$E_{c.m.}$ (GeV)	σ (μb)
1.60–1.70	2465 ± 564
1.70–1.80	3602 ± 619
1.80–1.85	2888 ± 419
1.85–1.875	1586 ± 313
1.875–1.90	1597 ± 292
1.90–1.925	1171 ± 230
1.925–1.95	1009 ± 212
1.95–1.975	756 ± 162
1.975–2.00	777 ± 177
2.00–2.025	1048 ± 180
2.025–2.05	990 ± 175
2.05–2.075	1038 ± 194
2.075–2.10	775 ± 142
2.10–2.125	966 ± 145
2.125–2.15	605 ± 107
2.15–2.175	478 ± 95.6
2.175–2.20	548 ± 106
2.20–2.225	559 ± 97.4
2.225–2.25	364 ± 64.7
2.25–2.275	603 ± 87.6
2.275–2.30	498 ± 78.3
2.30–2.325	290 ± 58.6
2.325–2.35	427 ± 64.0
2.35–2.40	302 ± 37.5
2.40–2.45	296 ± 35.1
2.45–2.50	287 ± 33.9
2.50–2.60	211 ± 19.9
2.60–2.70	188 ± 16.4
2.70–2.80	136 ± 15.2
2.80–2.90	123 ± 13.0
2.90–3.00	115 ± 13.1

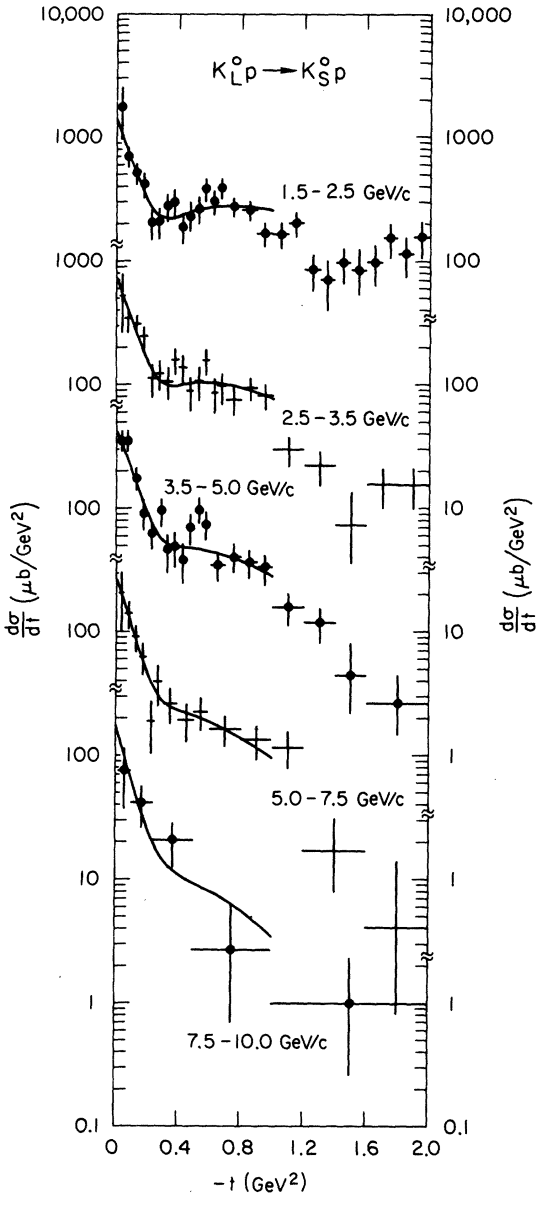

FIG. 4. Forward differential cross sections for $K_L^0 p \to K_S^0 p$ in five momentum intervals between 1.5 and 10.0 GeV/c. The solid curves are from a fit using the dual absorptive model described in Sec. IV E.

for five momentum intervals between 1.5 and 10 GeV/c. The data are strongly forward peaked, with a distinct break in the cross section slope at $|t| \sim 0.3$ GeV^2. No other fixed-t structure is observed in the differential cross section for $|t| \lesssim 2$ GeV^2.

The forward peaking in the $K_L^0 p \to K_S^0 p$ cross section indicates that the s-channel helicity-nonflip amplitude is large for this reaction. By comparison, in the dominantly helicity-flip reaction $\pi^- p \to \pi^0 n$ the cross section actually decreases in the very forward direction, and has a significant minimum near $|t| \sim 0.6$ GeV^2. This latter feature has been offered as confirmation for the Regge signature factor in scattering amplitudes:

$$f_{\Delta\lambda}(t) = \tilde{f}_{\Delta\lambda}(t)(1 - e^{-i\pi\alpha_\rho(t)}) . \tag{8}$$

Since a linear trajectory $\alpha_\rho(t)$ crosses zero near $|t| \sim 0.6$ GeV^2, ρ-exchange dominated cross sections are predicted to have a minimum near this value of momentum transfer, in agreement with the $\pi^- p \to \pi^0 n$ data. Although $\alpha_\omega(t)$ is thought to be essentially equal to $\alpha_\rho(t)$, no similar minimum is observed in the $K_L^0 p \to K_S^0 p$ cross section (see Fig. 4). Further comparisons of the $K_L^0 p \to K_S^0 p$ and $\pi^- p \to \pi^0 n$ differential cross sections are presented in Section IV E.

C. Phase of the $K_L^0 p \to K_S^0 p$ forward amplitude

In the very forward direction the s-channel helicity-flip amplitude must vanish to conserve angular momentum. Thus at $t = 0$ the helicity-nonflip amplitude provides the only contribution to the differential cross section. Since the imaginary part of this amplitude is determined by $\Delta\sigma_{K^\pm n}^{\text{tot}}$ [see Eq. (4)], it is possible to evaluate the phase of the forward amplitude:

$$\phi = \tan^{-1}(\text{Im} f_{\Delta\lambda=0} / \text{Re} f_{\Delta\lambda=0}) . \tag{9}$$

We first consider the imaginary part of the $K_L^0 p \to K_S^0 p$ amplitude. The optical theorem [Eq. (4)] indicates that the sign of the imaginary part is negative, that is, $\sigma_{K^- n}^{\text{tot}} > \sigma_{K^+ n}^{\text{tot}}$.[22-24] Evaluating the imaginary contribution to the forward $K_L^0 p \to K_S^0 p$ cross section, we obtain

$$\left(\frac{d\sigma}{dt}\right)_{\text{opt}} = \frac{1}{64\pi}\left(\frac{\Delta\sigma_{K^\pm n}^{\text{tot}}}{\hbar c}\right)^2 . \tag{10}$$

This then allows the ratio of the forward amplitude to be determined from the data:

$$\frac{\text{Re} f_{\Delta\lambda=0}}{\text{Im} f_{\Delta\lambda=0}} = \pm\left[\frac{(d\sigma/dt)_0}{(d\sigma/dt)_{\text{opt}}} - 1\right]^{1/2} . \tag{11}$$

The quadratic sign ambiguity in Eq. (11) can be resolved by recourse to dispersion relations.[1,25] An equivalent result is obtained using simple Regge theory where the signature factor gives the phase of the forward amplitude:

$$\left(\frac{\text{Re} f}{\text{Im} f}\right) \sim \tan\left(\frac{\pi\alpha(0)}{2}\right) . \tag{12}$$

For reasonable ω^0, ρ Regge trajectories, $\alpha(0)$ lies in the interval $0 < \alpha(0) < 1$ implying that $\text{Re} f / \text{Im} f$ is positive. The phase, ϕ, is thus defined to lie in the third quadrant.

TABLE VI. Forward differential cross sections: $(d\sigma/dt)(K_L^0 p \to K_S^0 p)$.

$-t$ interval (GeV^2) \ P_{lab} (GeV/c)	1.5–2.5	2.5–3.5	3.5–5.0	5–7.5	7.5–10
	$(d\sigma/dt)$ (μb/GeV^2)				
0.025–0.05	1754 ±795	520 ±255	359 ±172	209 ±109	75.1±37.6
0.05–0.10	702 ±138	344 ±79.8	353 ±73.6	141 ±35.4	
0.10–0.15	514 ±101	308 ±60.3	176 ±35.3	90.5±21.8	41.3±15.3
0.15–0.20	413 ±89.2	243 ±51.7	91.8±24.4	61.9±18.1	
0.20–0.25	207 ±58.9	111 ±31.6	63.7±18.1	18.9±8.6	
0.25–0.30	210 ±59.6	122 ±33.5	96.0±24.0	39.3±14.4	20.6±8.2
0.30–0.35	275 ±67.0	105 ±29.9	46.1±15.6	26.0±8.1	
0.35–0.40	302 ±73.7	158 ±37.5	48.5±15.6		
0.40–0.45	187 ±50.9	136 ±34.7	38.4±13.7	19.2±6.5	
0.45–0.50	234 ±56.3	88.2±27.0	69.0±18.7		
0.50–0.55	263 ±63.4	106 ±32.3	98.3±22.5	22.4±6.6	$2.7^{+3.6}_{-2.0}$
0.55–0.60	384 ±80.7	155 ±36.3	74.6±19.0		
0.60–0.65	299 ±66.8	85.5±27.4	34.4±9.0	16.3±4.5	
0.65–0.70	393 ±76.8	96.5±28.2			
0.70–0.80	275 ±47.2	74.7±18.0	40.3±10.5		
0.80–0.90	257 ±44.0	93.9±19.7	36.6±9.6	13.2±4.0	
0.90–1.00	166 ±34.8	80.9±18.5	32.8±8.9		
1.00–1.10	164 ±38.6	29.6±7.8	15.8±4.4	11.5±3.9	$0.98^{+1.32}_{-0.72}$
1.10–1.20	202 ±44.0				
1.20–1.30	84.2±27.7	21.9±6.7	11.7±3.7	$1.7^{+1.4}_{-0.9}$	
1.30–1.40	69.8±30.1				
1.40–1.50	94.9±30.6	$7.3^{+6.0}_{-3.7}$	$4.4^{+3.6}_{-2.2}$		
1.50–1.60	83.0±29.4				
1.60–1.70	97.2±35.1	15.4±5.5	$2.6^{+1.8}_{-1.2}$	$0.41^{+1.00}_{-0.33}$	
1.70–1.80	151 ±46.5				
1.80–1.90	112 ±40.5	15.3±5.5			
1.90–2.00	155 ±51.5				

The $K_L^0 p \to K_S^0 p$ cross sections are extrapolated to $t=0$ using the exponential parameterization

$$\frac{d\sigma}{dt} = \left(\frac{d\sigma}{dt}\right)_0 e^{bt} \tag{13}$$

in the momentum-transfer interval $0.025 \leq |t| \leq 0.25$ GeV^2. The forward differential cross sections are determined in five momentum intervals between 1.5 and 10 GeV/c. The resulting cross sections and slopes are shown in Figs. 5 and 6, and recorded in Table VII.

Previous experimental results[1-3,9,11] on the forward $K_L^0 p \to K_S^0 p$ cross section are also included in Fig. 5. Of these, the experiments of Darriulat *et al.*,[1] Buchanan *et al.*,[2] and Birulev *et al.*[3] are K_S^0 coherent-regeneration experiments measuring the $K_L^0 p \to K_S^0 p$ amplitude only at $t=0$. This technique exploits the observed interference in the proper time distribution of $\pi^+\pi^-$ decays of both K_S^0 and K_L^0 mesons to determine the magnitude and the phase of the forward $K_L^0 p \to K_S^0 p$ scattering amplitude. Good agreement is found between the present extrapolations of the $K_L^0 p \to K_S^0 p$ cross section and the results of the coherent-regeneration experiments.

We note that the forward cross section data are well described by the power-law form

$$\left(\frac{d\sigma}{dt}\right)_0 = A p_{lab}^{-n_0} . \tag{14}$$

Values of these parameters determined in several different momentum intervals are recorded in Table VIII. The curve in Fig. 5 results from the parametrization ($n_0 = 1.40$) of the $K_L^0 p \to K_S^0 p$ data above 2.5 GeV/c.[26]

Values for $(d\sigma/dt)_{opt}$, obtained from $\Delta\sigma_{K^\pm n}$ [see Eq. (10)], are shown in Fig. 7. The uncertainties in the cross-section differences are calculated summing the $K^\pm n$ cross section errors in quadrature. For the data of Ref. 22 a 2% systematic normalization uncertainty is included in both the $K^+ n$ and $K^- n$ data. Systematic uncertainties are not included for the Galbraith *et al.*[23] or the Denisov *et al.*[24] data, where the statistical errors are already large.[27]

Data on both $K^\pm n$ total cross sections exist below 3.3 GeV/c and above 6 GeV/c. To obtain estimates of the $K^\pm n$ cross-section differences in the momentum interval 1.5 to 10 GeV/c two procedures are used. Between 1.5 and 2.5 GeV/c the

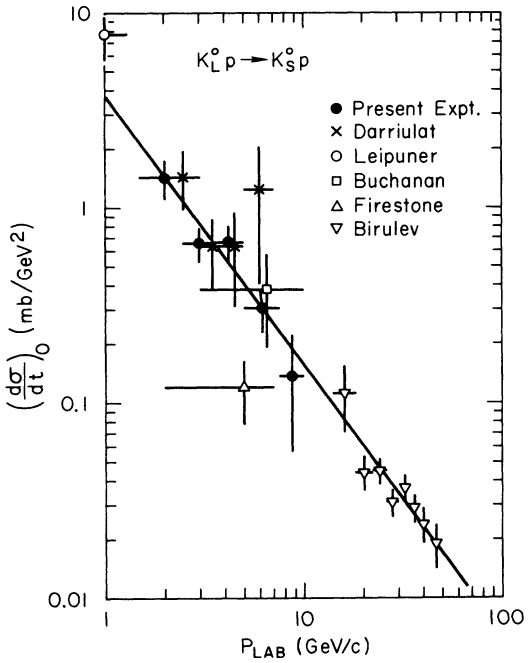

FIG. 5. Differential cross section at $t=0$ for $K_L^0 p \rightarrow K_S^0 p$. The solid points, determined by exponential extrapolation of the forward differential cross sections, are from the present experiment. Data from Refs. 1–3, 9, and 11 are also included. The solid curve is a parameterization of the data above 2.5 GeV/c with the form $(d\sigma/dt)_0 = A p_{\rm lab}^{\ -n_0}$.

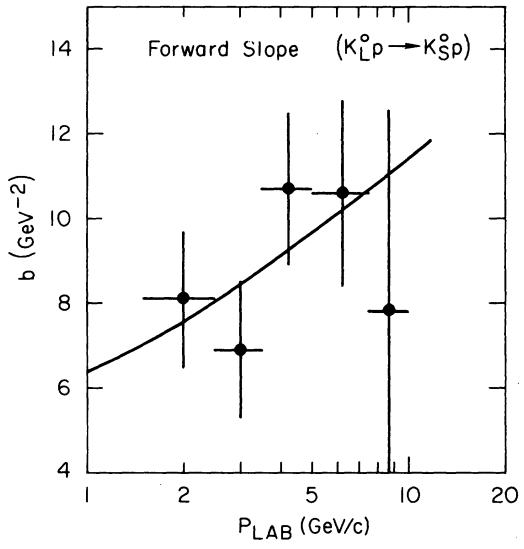

FIG. 6. Exponential slopes of the forward $K_L^0 p \rightarrow K_S^0 p$ differential cross section [see Eq. (13)] determined in the momentum-transfer interval $0.025 \leq |t| \leq 0.25$ GeV². The curve is a simple Regge parameterization of the data: $b(s) = b_0 + 2\alpha' \ln s$.

$(d\sigma/dt)_{\rm opt}$ data are directly averaged for comparison with the $K_L^0 p \rightarrow K_S^0 p$ forward data. Above 2.5 GeV/c, the $(d\sigma/dt)_{\rm opt}$ data are fitted to the power-law form,

$$\left(\frac{d\sigma}{dt}\right)_{\rm opt} = B p_{\rm lab}^{\ -n_{\rm opt}}, \qquad (15)$$

giving $B = 1965 \pm 202$ μb/GeV² and $n_{\rm opt} = 1.32 \pm 0.06$, as shown by the curve in Fig. 7. This result is then used to determine the average $(d\sigma/dt)_{\rm opt}$ cross sections in the momentum intervals recorded in Table VII. Finally, the quoted errors in $(d\sigma/dt)_{\rm opt}$ are scaled by a factor of 2 to allow for possible uncertainties coming from our choice of averaging procedures.

The results for the ratio of real to imaginary parts of the forward amplitude, the phase, and the intercept of the effective Regge trajectory then follow from Eqs. (9)–(12) and are recorded in Table VII. The phase of the $K_L^0 p \rightarrow K_S^0 p$ scattering amplitude is plotted together with previous measurements[1–3] in Fig. 8. The data indicate that the phase, ϕ, has little or no energy dependence in

TABLE VII. Determination of the phase of the forward amplitude for $K_L^0 p \rightarrow K_S^0 p$.

$P_{\rm lab}$ (GeV/c)	Slope [a] (GeV^{-2})	$(d\sigma/dt)_0$ (μb/GeV²)	$(d\sigma/dt)_{\rm opt}$ [b] (μb/GeV²)	(ReA/ImA)	ϕ (degrees)	$\alpha(0)$
1.5–2.5	8.1 ± 1.6	1425 ± 282	663 ± 60.8	1.07 ± 0.23	−137.0 ± 6.9	0.52 ± 0.08
2.5–3.5	6.9 ± 1.6	646 ± 134	465 ± 55.3	0.62 ± 0.27	−122.0 ± 11.0	0.36 ± 0.12
3.5–5.0	10.7 ± 1.8	665 ± 138	294 ± 31.0	1.12 ± 0.25	−138.4 ± 7.1	0.54 ± 0.08
5.0–7.5	10.6 ± 2.2	305 ± 78	177 ± 18.8	0.85 ± 0.28	−130.4 ± 9.3	0.45 ± 0.10
7.5–10.0	7.8 ± 4.8	138 ± 82	112 ± 13.6	0.48 ± 0.77	−115.6 ± 36.0	0.29 ± 0.40
			Weighted average	0.92 ± 0.13	−133.9 ± 4.0	0.49 ± 0.05
			Birulev *et al.* (Ref. 3)		−132.3 ± 5.7	
			Combined data		−133.4 ± 3.3	

[a] Slopes are determined in the interval $0.025 \leq |t| \leq 0.25$ GeV².

[b] Optical points are determined by parameterizing the $K^{\pm}n$ total cross section differences $(d\sigma/dt)_{\rm opt} = [\Delta\sigma^{\rm tot}_{K^{\pm}n}/(64\pi)^{1/2}\hbar c]^2 = A p^{-n_{\rm opt}}$ and averaging this result in the appropriate momentum interval.

TABLE VIII. Energy dependence of the $K_L^0 p \to K_S^0 p$ forward cross section, $(d\sigma/dt)_0(K_L^0 p \to K_S^0 p) = A p^{-n_0}$.

Momentum interval (GeV/c)	A (μb/GeV^2)	n_0	Reference
1.5–10.0	3255 ± 988	1.33 ± 0.24	Present expt.
14–50	1118 ± 996	1.04 ± 0.26	Birulev *et al.* (Ref. 3)
1.5–50	3274 ± 607 [a]	1.36 ± 0.06 [a]	Present expt.
2.5–50	3082 ± 749	1.34 ± 0.08	+
3.5–50	4013 ± 1400	1.42 ± 0.11	Birulev *et al.* (Ref. 3)
2.5–50	3834 ± 476	1.40 ± 0.05	Present expt. + Refs. 1–3

[a] For the combined data samples, the uncertainties in the forward cross sections have been augmented by a 10% systematic uncertainty combined in quadrature.

the interval 1.5 to 50 GeV/c. The average values of ϕ from the present experiment, $\phi = -133.9 \pm 4.0°$, and from the Serpukhov results, $\phi = -132.3 \pm 5.7°$,[3] are in good agreement and are consistent with the constant phase $\phi = -133.4 \pm 3.3°$ for the combined data.

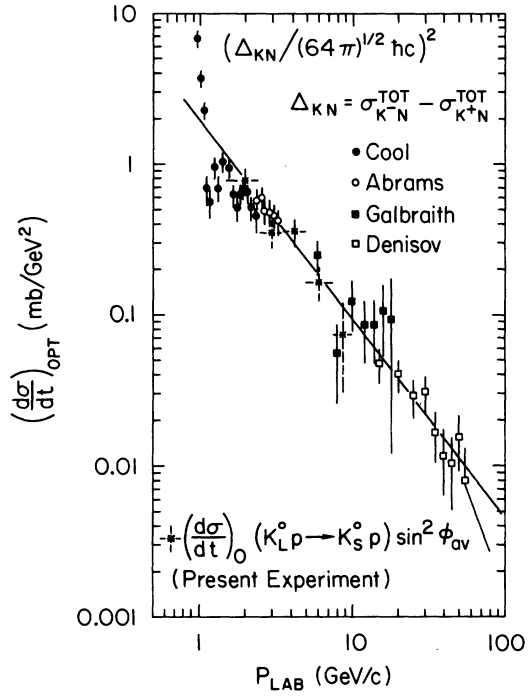

FIG. 7. The imaginary part of the $K_L^0 p \to K_S^0 p$ differential cross section at $t = 0$ determined from the optical theorem. The $K^{\pm} n$ total cross section data are from Refs. 22–24. The solid curve is a parameterization of the data above 2.5 GeV/c with the form $(d\sigma/dt)_{opt} = B p_{lab}^{-n_{opt}}$. The * points are found by scaling the forward $K_L^0 p \to K_S^0 p$ cross sections by $\sin^2\phi_{av}$, where ϕ_{av} is the average phase of the forward cross section (see Sec. IV C).

Recently the possibility has been suggested[28] that the value of the $K_L^0 \to \pi^+\pi^-$ decay parameter η_{+-} is different from the previously accepted value.[7] A change in η_{+-} could potentially alter the results of the K_S^0 coherent-regeneration experiments, and in particular the highest-energy (Serpukhov) data. However, the agreement of the present experiment with the coherent-regeneration results in the same momentum interval (see Figs. 5 and 8) suggests that the existing K_S^0 regeneration analyses are correct or insensitive to the possible change in η_{+-}. A further check is provided by the consistency of the phase determined directly from the K_S^0 coherent-regeneration experiments with the phase determined using their values of $(d\sigma/dt)_0$ together with Eqs. (9)–(11). To

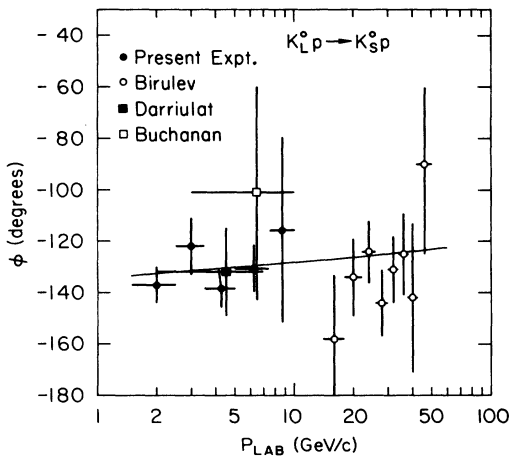

FIG. 8. Phase of the $K_L^0 p \to K_S^0 p$ scattering amplitude at $t = 0$. The ● data are from the present experiment. Results from K_S^0 coherent-regeneration experiments, Refs. 1–3, are also included. The curve shows the phase at $t = 0$ resulting from the power-law fits displayed in Figs. 5 and 7.

illustrate this comparison the solid curve in Fig. 8 shows the phase resulting from the p_{lab}^{-n} parametrizations of $(d\sigma/dt)_0$ and $(d\sigma/dt)_{\text{opt}}$ for $p_{\text{lab}} \geq 2.5$ GeV/c [see Eqs. (14) and (15)]. Although the slight inequality of n_0 and n_{opt} does predict a small change in ϕ with energy, it is clear that the values of ϕ obtained in this manner are consistent with all the K_S^0 coherent-regeneration data.

Having determined that the phase of the forward $K_L^0 p \to K_S^0 p$ amplitude is approximately constant, the average phase from the present experiment, $\phi = -133.9 \pm 4.0°$ is used to evaluate the contribution of the imaginary part of the forward cross section for our data. Thus our $(d\sigma/dt)_0$ data have been scaled by the factor $\sin^2\phi_{\text{av}}$ and plotted with dashed error bars in Fig. 7 to illustrate the common energy dependence of the $(d\sigma/dt)_0$ and $(d\sigma/dt)_{\text{opt}}$ data.

The intercepts of the ω^0, ρ Regge trajectory calculated from the present data [see Eq. (12)] are given in Table VII and yield the average value $\alpha(0) = 0.49 \pm 0.05$. The forward differential cross section for $\pi^- p \to \pi^0 n$,[29,30] and the total cross section differences, $\Delta\sigma_{\pi^\pm p}^{\text{tot}}$,[24] can be used in an analogous manner to determine the phase of the forward amplitude and therefore the ρ Regge trajectory, $\alpha_\rho(0)$. These latter data indicate that $\alpha_\rho(0)$ is almost independent of momentum, and has a value $\alpha_\rho(0) \sim 0.56$,[31] in the momentum interval spanned by our $K_L^0 p \to K_S^0 p$ data. The phases of the forward $K_L^0 p \to K_S^0 p$ and $\pi^- p \to \pi^0 n$ scattering amplitudes are similar therefore, and in agreement with the canonical value for the ω^0, ρ Regge intercept, $\alpha(0) \sim 0.5$.

D. Energy dependence of the $K_L^0 p \to K_S^0 p$ differential cross section

Simple Regge theory predicts that for reactions with only one (or two exchange-degenerate) t-channel Regge exchange(s) the cross section is proportional to

$$\frac{d\sigma}{dt}(s,t) \propto \frac{s^{2\alpha(t)}}{p_{\text{lab}}^{\,2}}\,, \tag{16}$$

where $\alpha(t)$ is the appropriate Regge trajectory. For ω^0 or ρ exchange, $\alpha(t)$ is approximately of the form

$$\alpha(t) = 0.5 + \alpha' t\,, \tag{17}$$

with $\alpha' \sim 1$ GeV^2.

Thus, if the forward differential cross sections are approximately exponential in momentum transfer, Eq. (16) predicts an increase in the forward slopes with energy:

$$\frac{d\sigma}{dt} = \left(\frac{d\sigma}{dt}\right)_0 \exp[(b_0 + 2\alpha' \ln s)t]\,. \tag{18}$$

The forward slopes for $K_L^0 p \to K_S^0 p$ plotted in Fig. 6 are consistent with an increase in the slopes with increasing momentum. Parameterizing the energy dependence of the slopes as in Eq. (18), we obtain $b_0 = 3.1 \pm 4.5$ GeV^{-2} and $\alpha' = 1.4 \pm 1.1$ GeV^{-2}, where the large uncertainties result in part from the parameters b_0 and α' being highly correlated.

Alternatively, the data can be parameterized with the form of Eq. (16); $\alpha(t)$ can then be directly determined as a function of momentum transfer. Tabular results from fits of our $K_L^0 p \to K_S^0 p$ data to Eq. (16), and the alternate forms

$$\frac{d\sigma}{dt} \propto p_{\text{lab}}^{\,2\alpha(t)-2} \tag{19a}$$

and

$$\frac{d\sigma}{dt} \propto \frac{(-u)^{2\alpha(t)}}{p_{\text{lab}}^{\,2}} \tag{19b}$$

are recorded in Table IX. The values of $\alpha(t)$ are observed to be only slightly different in the three parameterizations.

For uniformity of comparison with other analyses, the $\alpha(t)$ determined from Eq. (19a) are plot-

TABLE IX. Effective Regge trajectory, α_{eff}, for $K_L^0 p \to K_S^0 p$. Columns (a), (b), and (c) give α_{eff} determined using Eqs. (19a), (16), and (19b), respectively. To determine u for the purpose of our maximum-likelihood fits we use $u = \Sigma m_i^2 - s - \langle t \rangle$, where $\langle t \rangle$ is the average momentum transfer for the events in the given $|t|$ interval.

$\lvert t\rvert$ interval (GeV)^2	Momentum interval (GeV/c)	(a) α_{eff}	(b) α_{eff}	(c) α_{eff}
0.025–0.10	3–8	0.26 ± 0.18	0.30 ± 0.19	0.23 ± 0.15
0.10–0.20	3–8	0.14 ± 0.18	0.16 ± 0.20	0.12 ± 0.15
0.20–0.40	3–8	−0.08 ± 0.20	−0.09 ± 0.22	−0.07 ± 0.16
0.40–0.60	3–7	−0.02 ± 0.22	−0.03 ± 0.25	−0.01 ± 0.18
0.60–0.80	3–7	−0.14 ± 0.29	−0.16 ± 0.33	−0.11 ± 0.22
0.80–1.20	3–7	−0.25 ± 0.23	−0.28 ± 0.26	−0.19 ± 0.17
1.20–2.00	3–6	−0.97 ± 0.45	−1.14 ± 0.53	−0.62 ± 0.30

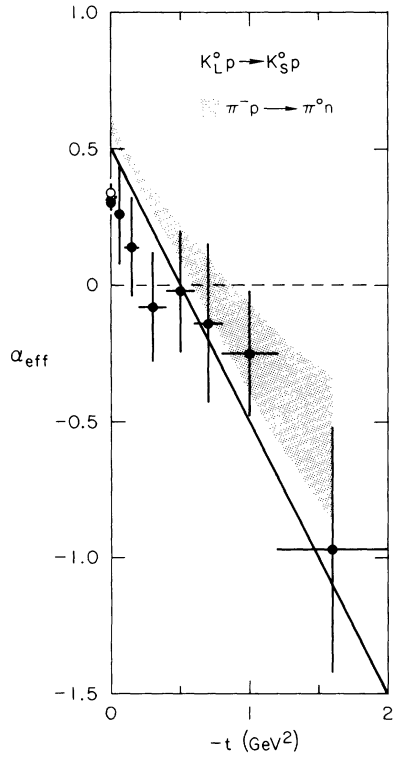

FIG. 9. Regge trajectory for $K_L^0 p \to K_S^0 p$ data resulting from a parameterization of the data with the form $d\sigma/dt(s,t) \propto p_{lab}{}^{2\alpha(t)-2}$. The points at $t<0$ are from the present experiment; the solid point at $t=0$ includes all the data (Refs. 1–3) above 2.5 GeV/c. The energy dependence of the imaginary part of the forward cross section (see Fig. 7) is shown by the open circle at $t=0$. The shaded region represents the results of a similar analysis of $\pi^- p \to \pi^0 n$ scattering (see Ref. 32). The solid curve depicts the canonical ω^0, ρ Regge trajectory, $\alpha(t) = 0.5 + t$.

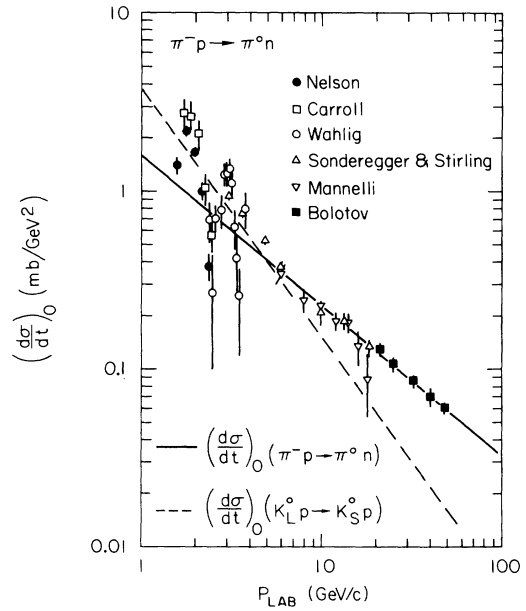

FIG. 10. The differential cross sections at $t=0$ for $\pi^- p \to \pi^0 n$ (see Ref. 30). The solid curve is a parametrization of the data above 5 GeV/c with form $(d\sigma/dt)_0 = A p_{lab}{}^{-n}$ (see Ref. 29). The dashed curve represents the $K_L^0 p \to K_S^0 p$ forward cross sections from Fig. 5.

ted in Fig. 9. The points for $t<0$ are from the present experiment; however, the solid point at $t=0$ is obtained using all the data above 2.5 GeV/c (see Table VIII). In addition, the energy dependence of the contribution of the imaginary part of the forward cross section (from the $\Delta\sigma_{K^\pm n}^{tot}$ data) has been plotted as the open point in Fig. 9. For comparison the canonical ω^0, ρ Regge trajectory, $\alpha(t) = 0.5 + t$, is shown as the solid line in Fig. 9. Approximate agreement is observed between the $K_L^0 p \to K_S^0 p$ data and the linear Regge trajectory, except near $|t| \approx 0$.

Interestingly, the value for $\alpha(0)$ determined from the energy dependence of the forward cross sections, $\alpha(0) = 0.30 \pm 0.03$, is in substantial disagreement with the value determined from the phase of the forward amplitude, $\alpha(0) = 0.49 \pm 0.05$. This result indicates a failure of the Regge phase-energy relation. Similar disagreements with the Regge predictions for helicity-nonflip amplitudes at momentum transfers, $t<0$, have been observed in the πN amplitude analyses at 6 GeV/c.[19–21]

For comparison with the present results, the ρ Regge trajectory derived from $\pi^- p \to \pi^0 n$ data[32] is shown shaded in Fig. 9. Since ω^0 and ρ Regge trajectories are essentially exchange-degenerate for $t>0$, the trajectories are expected to be nearly equal in the physical scattering region, $t \leq 0$. This is seen to be true for $|t| \gtrsim 0.4$ GeV^2, however the $K_L^0 p \to K_S^0 p$ data are systematically lower in the very forward direction. In particular, at $t=0$,

$$\alpha(0)_{K_L^0 p \to K_S^0 p} = 0.30 \pm 0.03,$$

whereas

$$\alpha(0)_{\pi^- p \to \pi^0 n} = 0.58 \pm 0.02.^{29}$$

This result has a direct bearing on the SU(3) relations in Eq. (3). For t-channel exchange models satisfying factorization and having exchange-degenerate ρ and ω^0 trajectories, the $K_L^0 p \to K_S^0 p$ and $\pi^- p \to \pi^0 n$ cross sections are predicted to have the same energy dependence, and to be simply related by the constant, F, in Eq. (3). A direct comparison of the $\pi^- p \to \pi^0 n$,[29,30] and $K_L^0 p \to K_S^0 p$ forward cross sections are shown in Fig. 10, where the dashed curve represents the

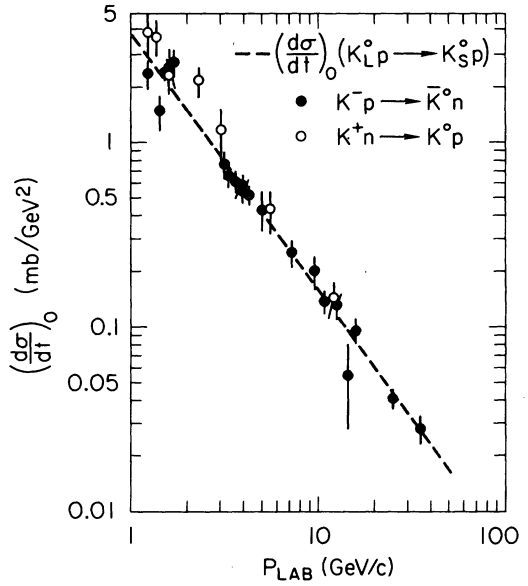

FIG. 11. The differential cross section at $t=0$ for KN charge-exchange scattering (see Ref. 33). The dashed curve represents the $K_L^0 p \rightarrow K_S^0 p$ forward cross sections from Fig. 5.

$K_L^0 p \rightarrow K_S^0 p$ data (see Fig. 5). Clearly, a fixed ratio between these cross sections does not exist, implying that the simple picture given by Eq. (3) is incorrect, or at least incomplete.

Since ω^0 and ρ exchanges dominate $K_L^0 p \rightarrow K_S^0 p$ and $\pi^- p \rightarrow \pi^0 n$ scattering, respectively, one explanation for the dissimilarity in the energy behavior of the forward cross sections is simply that ω^0 and ρ exchange amplitudes have intrinsically different energy dependences. However, as an additional check the forward cross sections for $K_L^0 p \rightarrow K_S^0 p$ and KN charge-exchange scattering[33] (having ρ and A_2 t-channel quantum numbers) are compared in Fig. 11. In contrast with the result in Fig. 10, the $K_L^0 p \rightarrow K_S^0 p$ and KN charge-exchange forward cross sections in Fig. 11 are observed to agree in magnitude (a mere coincidence?) as well as in energy dependence. These results then suggest that ω^0, ρ, and A_2 exchange amplitudes are consistent with exchange degeneracy (equal energy dependence), but that t-channel factorization is broken for reactions with different particles in the s channel. Absorption or direct-channel effects are thought to be important for helicity-nonflip amplitudes for $t<0$;[34,35] the present result suggests that direct-channel effects are also important at $t=0$.

The approximate energy independence of the phases of the forward scattering amplitudes for $K_L^0 p \rightarrow K_S^0 p$ and $\pi^- p \rightarrow \pi^0 n$, combined with the observed inequality of the energy dependence of their forward cross sections, then implies that the energy dependences of the total cross section differences, $\Delta\sigma_{K^\pm n}^{\text{tot}}$ and $\Delta\sigma_{\pi^\pm p}^{\text{tot}}$ [see Eq. (4)], must also be unequal. This is experimentally the case[24]; $\Delta\sigma_{\pi^\pm p}^{\text{tot}}$ decreases with energy substantially more slowly than $\Delta\sigma_{K^\pm n}^{\text{tot}}$. Similar discrepancies between the energy dependence of forward cross sections are also observed in other channels.[36]

E. Amplitude structure of $K_L^0 p \rightarrow K_S^0 p$ forward cross sections

Amplitude analyses of $\pi N \rightarrow \pi N$ scattering data have recently been completed at 6 GeV/c.[19-21] One result is the essentially model-independent determination of the t-channel isospin-one "ρ"-exchange amplitude. Assuming that ρ and ω^0 vector-exchange amplitudes have similar structures (as a function of momentum transfer), the ρ amplitudes from πN scattering should then be simply related by a multiplicative factor, $a_{\Delta\lambda}$, to the $\rho+\omega^0$ amplitude in $K_L^0 p \rightarrow K_S^0 p$ scattering:

$$f_{\Delta\lambda}(K_L^0 p \rightarrow K_S^0 p) = a_{\Delta\lambda} V_{\Delta\lambda}, \tag{20}$$

where $\Delta\lambda$ is the net helicity flip in the reaction.

In the following analysis the $V_{\Delta\lambda}$ are chosen to be the Saclay $I_t=1$ amplitudes[20] [see Eq. (3)] and the coefficients in Eq. (20) are obtained by fitting the sum of the πN amplitudes to the $K_L^0 p \rightarrow K_S^0 p$ differential cross section in the momentum-transfer interval $0.025 \leq |t| \leq 0.30$ GeV^2. Fits to the $K_L^0 p \rightarrow K_S^0 p$ data in larger momentum-transfer intervals disagree substantially with the data near $t=0$ and are not considered. The analysis of the 5- to 7.5-GeV/c $K_L^0 p \rightarrow K_S^0 p$ data is shown in Fig. 12. The solid curve in Fig. 12(a) represents the best fit of the Saclay amplitudes[20] to the $K_L^0 p \rightarrow K_S^0 p$ data; the shaded region in Fig. 12(a) displays the uncertainties in the structure of the Saclay amplitudes. For completeness, the polarization prediction for this solution is shown in Fig. 13; again the shaded region reflects the uncertainties on the πN amplitudes.

The coefficients corresponding to the fit in Fig. 12(a) are $a_{\Delta\lambda=0}=1.85\pm0.77$ and $a_{\Delta\lambda=1}=-0.48\pm0.09$. This result is in approximate agreement with the SU(3) predictions, $a_{\Delta\lambda}=(2F-1)$ of Eqs. (3) and (5). We note that the sign of the $a_{\Delta\lambda=1}$ coefficient has been chosen to agree with the SU(3) prediction. Experimentally, this sign could be determined from the polarization in $K_L^0 p \rightarrow K_S^0 p$ scattering.

The comparison of the Saclay amplitudes to the $K_L^0 p \rightarrow K_S^0 p$ data [Fig. 12(a)] indicates that the πN amplitudes predict too small a cross section for $|t| \gtrsim 0.3$ GeV^2. The recent Argonne πN amplitude analysis,[21] which has a smaller $I_t=1$ helicity-nonflip amplitude than the Saclay solution in this momentum transfer region, is in even greater dis-

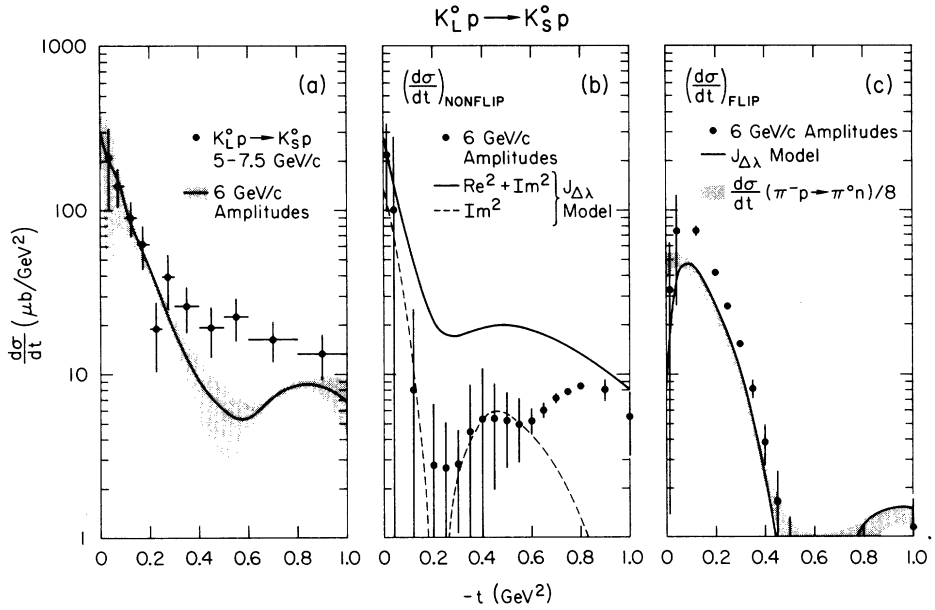

FIG. 12. Comparison of s-channel helicity amplitudes with the $K_L^0 p \to K_S^0 p$ data in the interval 5 to 7.5 GeV/c. The differential cross section is shown in (a); the helicity-nonflip and -flip contributions to the cross section are shown in (b) and (c), respectively. The curves are explained in Sec. IV E.

agreement with the $K_L^0 p \to K_S^0 p$ differential cross section.

To investigate the discrepancy between the $K_L^0 p \to K_S^0 p$ differential cross section and the πN amplitude results, the contribution of the separate helicity-nonflip and -flip amplitudes to the cross section are shown in Figs. 12(b) and 12(c), respectively. In these figures the Saclay amplitudes are simply scaled by the appropriate $a_{\Delta\lambda}$ coefficient, Eq. (20). The SU(3) prediction, Eq. (7), for the helicity-flip contribution to the $K_L^0 p \to K_S^0 p$ cross section is shown as the shaded curve in Fig. 12(c). Thus the helicity-nonflip amplitude is predicted to dominate the differential cross section in the very forward direction, $|t| < 0.05$ GeV^2 and for $|t| \gtrsim 0.4$ GeV^2, whereas at intermediate values of momentum transfer, $0.05 < |t| < 0.4$ GeV^2, the helicity-flip amplitude is the most important. The predicted composition of the differential cross section is therefore quite complex.

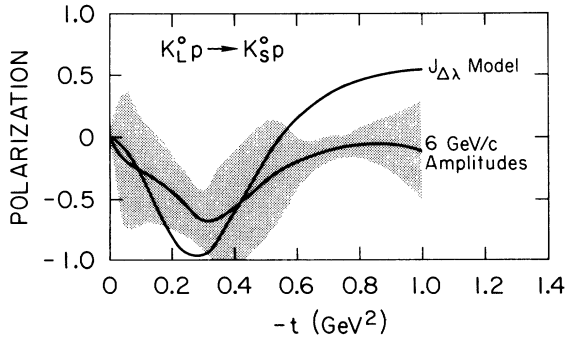

FIG. 13. Predicted polarization for $K_L^0 p \to K_S^0 p$ scattering at 6 GeV/c. The curves are discussed in Sec. IV E.

Interestingly, in the momentum-transfer interval where the largest discrepancy exists between the $K_L^0 p \to K_S^0 p$ data and the πN amplitudes, the cross section is dominated by the helicity-nonflip amplitude. Since ω^0 exchange is thought to dominate the helicity-nonflip amplitude [see Eqs. (3) and (5)], an intrinsic difference in the structure of ρ and ω^0 exchange amplitudes could account for the discrepancy observed in Fig. 12(a). Alternatively, helicity-nonflip amplitudes are thought to be substantially influenced by direct channel or absorptive effects. Thus while the ρ and ω^0 amplitudes may have a similar structure in a given reaction, these amplitudes, and in particular the ρ-exchange amplitude, may be significantly different in πN and KN channels.

Assuming that it is the helicity-nonflip amplitude that differs substantially between KN and πN reactions,[37] a good description of the $K_L^0 p \to K_S^0 p$ data can in fact be obtained using a parameterization that allows the real part of the helicity-nonflip amplitude to differ significantly between $K_L^0 p \to K_S^0 p$ and $\pi^- p \to \pi^0 n$ reactions. The amplitudes have the form

$$\mathrm{Im}f_{\Delta\lambda=0}(s,t)=g_0\left(\frac{s}{s_0}\right)^{\alpha(t)+\Delta\alpha}e^{At}J_0(r\sqrt{-t}),$$

$$\mathrm{Re}f_{\Delta\lambda=0}(s,t)=g_0\left(\frac{s}{s_0}\right)^{\alpha(t)+\Delta\alpha}\times e^{At}[(1+at+bt^2)e^{Bt}]\tan\tfrac{1}{2}\pi\alpha(0), \quad (21)$$

and

$$f_{\Delta\lambda=1}=g_1\left(\frac{s}{s_0}\right)^{\alpha(t)+\Delta\alpha}e^{At}J_1(r\sqrt{-t})[\tan\tfrac{1}{2}\pi\alpha(t)+i],$$

as suggested by the dual absorptive model (DAM) of Harari,[34,38] and previously discussed in Ref. 39. In Eq. (21) $\alpha(t)$ is the ω^0, ρ Regge trajectory and s_0 is set to 1 GeV^2. The parameters obtained by fitting the $K_L^0 p \to K_S^0 p$ data are given in Table X; the curves in Fig. 4 show the comparison of the DAM to the $K_L^0 p \to K_S^0 p$ data. The contributions of the helicity-nonflip and -flip DAM amplitudes to the 5–7.5 GeV/c data are shown in Figs. 12(b) and 12(c) and the polarization prediction is shown in Fig. 13.

We note that the DAM, the πN amplitudes, and the SU(3) prediction [Eq. (7)] are in approximate agreement for the helicity-flip contribution to the cross section, Fig. 12(c). In contrast, the DAM helicity-nonflip amplitude is much larger than the πN amplitude result for $|t| \gtrsim 0.1$ GeV^2. In particular for $0.1 \lesssim |t| \lesssim 0.6$ GeV^2 the magnitude of the imaginary part of the DAM nonflip amplitude, shown dashed in Fig. 12(b), is sufficient to duplicate the πN amplitude result which itself is predominantly imaginary in this momentum-transfer interval.[19–21] Thus the difference in the $K_L^0 p \to K_S^0 p$ and πN amplitudes is attributed, in the DAM parameterization, to the much larger real part in the helicity-nonflip amplitude in the $K_L^0 p \to K_S^0 p$ reaction.

TABLE X. Dual absorptive model parameters for fit to $K_L^0 p \to K_S^0 p$ forward cross sections.

Reaction	$K_L^0 p \to K_S^0 p$	$\pi^- p \to \pi^0 n$ [a]
r (GeV^{-1})	5.19	5.19
A (GeV^{-2})	−0.88	−0.93
g_0	−19.0	−15.0
g_1	17.0	−30.9
a (GeV^{-2})	2.97	5.56
b (GeV^{-4})	8.79	10.20
c (GeV^{-6})	···	5.22
B (GeV^{-2})	2.0	1.5
α' (GeV^{-2})	0.88	0.9
$\Delta\alpha$	−0.14	···

[a] Results from a similar comparison to $\pi^- p \to \pi^0 n$, Ref. 39.

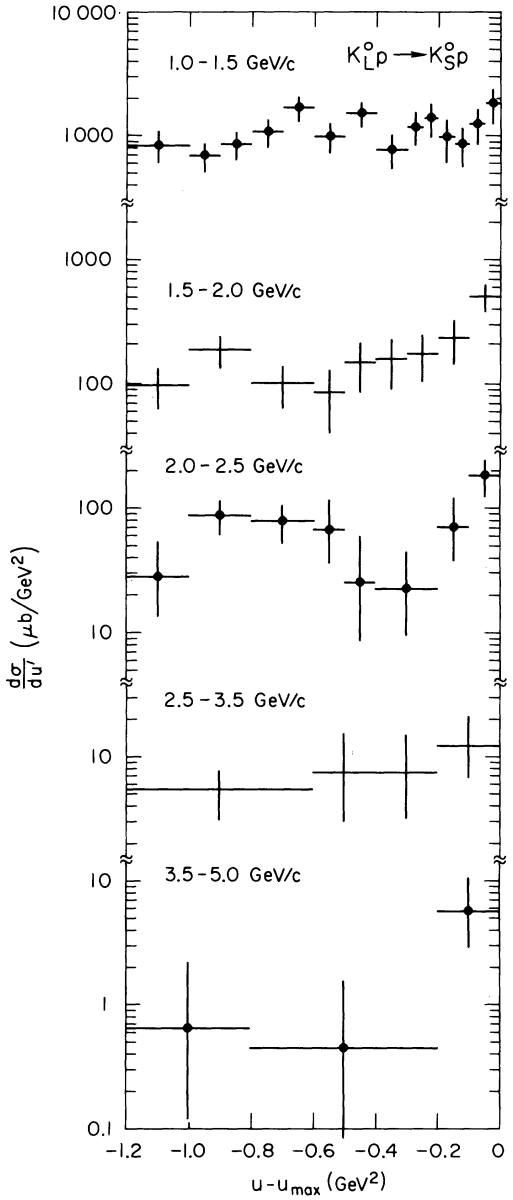

FIG. 14. Backward differential cross section for $K_L^0 p \to K_S^0 p$ in five momentum intervals between 1 and 5 GeV/c.

V. CROSS SECTIONS AT LARGE ANGLES

The analyses of our $K_L^0 p \to K_S^0 p$ backward scattering data and 90° scattering data[5] have been published previously. However, for completeness a summary is provided here, and the data are presented in tabular form for reference purposes.

Typically, scattering in the backward direction is discussed in terms of the possible u-channel exchanges. Reducing the $K_L^0 p \to p K_S^0$ scattering amplitudes into the states of well-defined strangeness

TABLE XI. Backward differential cross sections, $(d\sigma/du')(K_L^0 p \to pK_S^0)$.

P_{lab} (GeV/c)	1.0–1.5	1.5–2.0	2.0–2.5	2.5–3.5	3.5–5.0	5.0–7.5
$\langle u_{max} \rangle$ (GeV^2)	−0.110	−0.088	−0.073	−0.059	−0.044	−0.031
u' interval (GeV^2)	$(d\sigma/du')$ (μb/GeV^2)					
0–0.05	1872 ± 564	510 ± 126	185 ± 59.6	$12.3^{+8.9}_{-5.6}$	$5.6^{+4.7}_{-2.9}$	$0.93^{+2.26}_{-0.75}$
0.05–0.10	1265 ± 420					
0.10–0.15	874 ± 332	235 ± 84.7	$70.2^{+51.5}_{-32.4}$			
0.15–0.20	993 ± 377					
0.20–0.25	1400 ± 410	175 ± 70.4	$22.4^{+22.8}_{-12.9}$	$7.6^{+7.7}_{-4.4}$	$0.42^{+1.02}_{-0.34}$	<0.34
0.25–0.30	1197 ± 360					
0.30–0.40	777 ± 234	160 ± 68.8				
0.40–0.50	1512 ± 343	150 ± 64.8	$25.1^{+34.5}_{-16.6}$	$7.4^{+7.6}_{-4.3}$		
0.50–0.60	945 ± 259	$80.3^{+68.8}_{-41.7}$	$67.4^{+49.3}_{-31.0}$			
0.60–0.70	1651 ± 371	106 ± 38.2	78.7 ± 25.1	5.2 ± 2.2		
0.70–0.80	1024 ± 247					
0.80–0.90	895 ± 204	180 ± 50.9	86.9 ± 25.6		$0.62^{+1.50}_{-0.50}$	
0.90–1.0	664 ± 177					
1.0–1.2	828 ± 230	93.8 ± 33.5	$27.0^{+23.1}_{-14.0}$			

$$A_{K_L^0 p \to p K_S^0} = \tfrac{1}{2}(A_{K^0 p \to p K^0} - A_{\bar{K}^0 p \to p \bar{K}^0}),$$

we observe that the reaction $K^0 p \to pK^0$ allows only u-channel Σ exchanges, whereas the channel $\bar{K}^0 p \to p\bar{K}^0$ is exotic. Thus at sufficiently high energies the $K^0 p \to pK^0$ amplitude should dominate the $\bar{K}^0 p \to p\bar{K}^0$ amplitude, isolating the Σ-exchange contribution to the $K_L^0 p \to pK_S^0$ differential cross section:

$$\frac{d\sigma}{dt}(K_L^0 p \to pK_S^0) \xrightarrow[\text{large energy}]{} \frac{1}{4}\frac{d\sigma}{dt}(K^0 p \to pK^0).$$

Comparisons of the backward $K_L^0 p \to pK_S^0$ cross sections to backward $K^+ p \to pK^+$ scattering (where Λ and Σ exchanges occur in the u channel) and to the reaction $\pi^- p \to \Lambda^0 K^0$, which also isolates u-channel Σ exchange, are presented in Ref. 5.

To determine the cross sections at 180° ($u' = 0$), the $K_L^0 p \to pK_S^0$ data, shown in Fig. 14 and presented in Table XI, are parameterized with the form

$$\frac{d\sigma}{du'} = \left(\frac{d\sigma}{du'}\right)_0 e^{bu'}.$$

Momentum-transfer intervals are chosen consistent with the backward cross section being described by a single exponential. The u' intervals, the resulting slopes, and cross sections are recorded in Table XII. The $K_L^0 p \to pK_S^0$ slopes do vary substantially through the resonance region; however, the average slope below 5 GeV/c, $\langle b \rangle \sim 6$ GeV^{-2}, is in qualitative agreement with the slope for the reaction $\pi^- p \to \Lambda^0 K^0$, $\langle b \rangle = 5.5 \pm 0.5$ GeV^{-2}.[40] This slope is chosen therefore to determine the $K_L^0 p \to K_S^0 p$ backward cross section in the highest momentum interval (see Table XII), where there are insufficient data to determine a slope.

The energy dependence of the backward cross sections and the cross sections at 90° are pre-

TABLE XII. $K_L^0 p \to pK_S^0$ backward differential cross sections at 180° ($u = u_{max}$).

P_{lab} (GeV/c)	Momentum transfer interval u' (GeV^2)	Slope (GeV^{-2})	$(d\sigma/du')_{u'=0}$ (μb/GeV^2)	$(d\sigma/d\Omega)_{180°}$ (μb/sr)
1.0–1.5	0.0–0.15	8.3 ± 4.2	2345 ± 742	281 ± 89.0
1.5–2.0	0.0–0.3	5.7 ± 2.1	641 ± 187	121 ± 35.3
2.0–2.5	0.0–0.4	9.0 ± 2.6	277 ± 98.2	72.3 ± 25.6
2.5–3.5	0.0–0.6	1.7 ± 1.8	14.5 ± 7.9	5.4 ± 2.9
3.5–5.0	0.0–0.8	$5.0^{+3.2}_{-2.7}$	$6.8^{+5.1}_{-4.6}$	$3.8^{+2.8}_{-2.5}$
5.0–7.5	0.0–0.6	5.5 ± 0.5 [a]	$1.1^{+2.6}_{-0.9}$	$0.9^{+2.2}_{-0.8}$

[a] Slope value taken from the related reaction $\pi^- p \to \Lambda^0 K^0$.

sented in Tables XII and XIII, respectively. Both cross sections decrease by over three orders of magnitude between 1 and 7.5 GeV/c. In contrast the forward cross sections, Table VI, decrease by less than a factor of 10 in the same momentum interval.

The energy dependence of the 90° scattering cross sections is of particular interest since large transverse momentum reactions are potential probes of the hadronic structure at small distances.[41] Comparisons of the 90° data to parton-model predictions and to the predictions of single-particle inclusive cross sections are discussed in Ref. 5.

TABLE XIII. $K_L^0 p \to K_S^0 p$ cross section near 90°.

P_{lab} (GeV/c)	$(d\sigma/d\Omega)_{90°}$ [a] (μb/sr)	$(d\sigma/dt)_{90°}$ [a] (μb/GeV^2)
1.0–1.5	133 ±19.8	1104 ±165
1.5–2.0	35.6±5.6	190 ±29.9
2.0–2.5	10.0±2.3	38.6±9.0
2.5–3.5	4.52±0.84	12.3±2.3
3.5–5.0	$0.43^{+0.30}_{-0.19}$	$0.79^{+0.55}_{-0.35}$
5.0–7.5	<0.043 [b]	<0.051 [b]

[a] Determined in the center-of-mass scattering interval $-0.2 < \cos\theta < 0.2$.

[b] Cross-section upper bounds correspond to 85% confidence limit (1.9 events when no events were observed).

VI. SUMMARY AND CONCLUSIONS

Differential cross sections are presented for $K_L^0 p \to K_S^0 p$ scattering in several momentum intervals between 1 and 10 GeV/c. The general features of the data are the following:

(a) The differential cross sections show forward and backward peaks in all momentum intervals. In particular the strong forward peak indicates the importance of the s-channel helicity-nonflip scattering amplitude in $K_L^0 p \to K_S^0 p$.

(b) The energy dependence of the $K_L^0 p \to K_S^0 p$ cross section is approximately $\sigma \propto p_{\text{lab}}^{-2.1}$ in the interval 1 to 10 GeV/c. The energy dependence of the cross section at $t=0$ is more gradual however with $(d\sigma/dt)_0 \propto p_{\text{lab}}^{-1.33\pm0.24}$ for the present data, or $(d\sigma/dt)_0 \propto p_{\text{lab}}^{-1.40\pm0.05}$ for all data in the momentum interval 2.5 to 50 GeV/c.

(c) The phase of the $K_L^0 p \to K_S^0 p$ scattering amplitude at $t=0$ is consistent with being independent of energy: $\phi = -133.9 \pm 4.0°$ for the present data, and $\phi = -133.4 \pm 3.3°$ between 1.5 and 50 GeV/c.

(d) Expressing the energy dependence of the data in the form $(d\sigma/dt)(s,t) \propto p_{\text{lab}}^{2\alpha(t)-2}$, the Regge trajectory for the $K_L^0 p \to K_S^0 p$ data is in approximate agreement with the canonical ω^0, ρ trajectory, $\alpha(t) = 0.5 + t$, for $|t| \gtrsim 0.4$ GeV^2, but falls significantly below the prediction for $|t| < 0.4$ GeV^2. In addition the value at $t=0$, $\alpha(0) = 0.30 \pm 0.03$, is substantially different from the Regge-trajectory intercept determined from the phase of the forward amplitude, $\alpha(0) = 0.49 \pm 0.05$. This indicates a breaking of the Regge phase-energy relation at $t=0$.

(e) The $K_L^0 p \to K_S^0 p$ differential cross section has a distinct break at $|t| \sim 0.3$ GeV^2, but does not have a minimum at $|t| \sim 0.6$ GeV^2 in contrast with the pronounced dip observed in the related reaction $\pi^- p \to \pi^0 n$.

Comparisons of the energy dependences of the forward $K_L^0 p \to K_S^0 p$ and $\pi^- p \to \pi^0 n$ cross sections find a substantial disagreement: $\alpha(0)_{K_L^0 p \to K_S^0 p} = 0.30 \pm 0.03$, while $\alpha(0)_{\pi^- p \to \pi^0 n} = 0.58 \pm 0.02$.[29] A similar result is obtained by comparing only the imaginary parts of these cross sections, $\Delta\sigma^{\text{tot}}_{K^\pm n}$ and $\Delta\sigma^{\text{tot}}_{\pi^\pm p}$.[24] In contrast, the energy dependence of the forward cross sections for $K_L^0 p \to K_S^0 p$ and KN charge exchange are in good agreement. These comparisons suggest that direct-channel or absorption effects are breaking t-channel factorization for those reactions with different particles in the s channel.

The comparison of the $I_t = 1$ πN amplitude analysis results to the $K_L^0 p \to K_S^0 p$ differential cross section suggests that the helicity-nonflip amplitude for vector exchange is different for $\pi^- p \to \pi^0 n$ and $K_L^0 p \to K_S^0 p$ scattering. Since direct-channel effects are thought to be important for helicity-nonflip amplitudes, absorption may also explain the momentum-transfer-dependent differences between the $K_L^0 p \to K_S^0 p$ and $\pi^- p \to \pi^0 n$ differential cross sections.

ACKNOWLEDGMENTS

We wish to acknowledge the assistence provided by R. Watt and the crew of the SLAC 40-in. bubble chamber, by J. Brown and the scanning and measuring staff at SLAC, and by D. Johnson.

*Work supported by the U. S. Atomic Energy Commission.

†Now at Duke University, Durham, North Carolina.
‡Now at University of Toronto, Toronto, Canada.
§Now at University of Washington, Seattle, Washington.
‖Now at National Accelerator Lab, Batavia, Illinois.
**Now at Lawrence Berkeley Lab, Berkeley, California.
††Now at Purdue University, Lafayette, Indiana.

[1]P. Darriulat, C. Grosso, M. Holder, J. Pilcher, E. Radermacher, C. Rubbia, M. Scire, A. Staude, and K. Tittel, Phys. Lett. 33B, 433 (1970).
[2]C. D. Buchanan, D. J. Drickey, F. D. Rudnick, P. F. Shepard, D. H. Stork, H. K. Ticho, C.-Y. Chien, B. Cox, L. Ettlinger, L. Resvanis, R. A. Zdanis, E. Dally, E. Seppi, and P. Innocenti, Phys. Lett. 37B, 213 (1971).
[3]V. K. Birulev, V. Genchev, N. N. Govorun, T. S. Grigalashvili, B. N. Guskov, J. Hladky, I. M. Ivanchenko, V. D. Kekelidze, K. Kiss, V. G. Krivokhizhin, V. V. Kukhtin, M. F. Likhachev, E. Nagy, M. Nowak, A. Krokes, Yu. I. Salomatin, I. A. Savin, L. V. Silvestrov, V. E. Simonov, D. A. Smolin, G. G. Takhtanyshev, P. Todorev, L. Urban, A. S. Vovenko, G. Veszergomlsi, and J. Votruba, JINR report, 1972 (unpublished); Phys. Lett. 38B, 452 (1972).
[4]A preliminary report of the experiment is given by A. D. Brody *et al.*, Phys. Rev. Lett. 26, 1050 (1971).
[5]G. W. Brandenburg, W. B. Johnson, D. W. G. S. Leith, J. S. Loos, G. J. Luste, J. A. J. Matthews, K. Moriyasu, W. M. Smart, F. C. Winkelmann, and R. J. Yamartino, Phys. Rev. Lett. 30, 145 (1973); G. W. Brandenburg, W. B. Johnson, D. W. G. S. Leith, J. S. Loos, J. A. J. Matthews, F. C. Winkelmann, and R. J. Yamartino, Phys. Lett. 44B, 305 (1973).
[6]G. W. Brandenburg, A. D. Brody, W. B. Johnson, D. W. G. S. Leith, J. S. Loos, G. J. Luste, J. A. J. Matthews, K. Moriyasu, B. C. Shen, W. M. Smart, F. C. Winkelmann, and R. J. Yamartino, Phys. Rev. D 7, 708 (1973).
[7]Particle Data Group, Phys. Lett. 39B, 1 (1972).
[8]The results of the fit are $A = 1737\ \mu b/GeV^2$, $m = 0.732$ and $b_0 = 5.29\ GeV^{-2}$. The fit was fairly insensitive to the parameter b', which was therefore fixed to the reasonable Regge slope value $b' = 0.9\ GeV^{-2}$.
[9]L. B. Leipuner, W. Chinowsky, R. Crittenden, R. Adair, B. Musgrave, and F. T. Shively, Phys. Rev. 132, 2285 (1963).
[10]C. J. B. Hawkins, Phys. Rev. 156, 1444 (1967); D. Luers, I. S. Mittra, W. J. Willis, and S. S. Yamamoto, in *Proceedings of the Aix-en-Provence Conference on Elementary Particles, 1961* (Centre d'Etudes Nucleaires de Saclay, Gif-sur-Yvette, Seine et Oise, Saclay, France, 1961), p. 235; G. W. Meisner and F. S. Crawford, Phys. Rev. D 3, 2553 (1971).
[11]A. Firestone, J. K. Kim, J. Lach, J. Sandweiss, H. D. Taft, V. Barnes, H. W. J. Foelsche, T. Morris, Y. Oren, and M. Webster, Phys. Rev. Lett. 16, 556 (1966).
[12]V. N. Bolotov *et al.*, Phys. Lett. 38B, 120 (1971).
[13]V. N. Bolotov, M. I. Devishev, V. V. Isakov, D. B. Kakauridse, V. A. Kachanov, V. M. Kutin, Yu. D. Prokoshkin, E. A. Razuvaev, and V. K. Semenov, Serpukhov report, 1972 (unpublished).
[14]V. I. Belousov *et al.*, Phys. Lett. 43B, 76 (1973).
[15]A. Firestone, G. Goldhaber, A. Hirata, D. Lissauer, and G. H. Trilling, Phys. Rev. Lett. 25, 958 (1970).
[16]V. Barger and D. Cline, Phys. Rev. Lett. 24, 1313 (1970).
[17]F. J. Gilman, Phys. Rev. 171, 1453 (1968).
[18]A. D. Martin, C. Michael, and R. J. N. Phillips, Nucl. Phys. B43, 13 (1972).
[19]F. Halzen and C. Michael, Phys. Lett. 36B, 367 (1971).
[20]G. Cozzika, Y. Ducros, A. Gaidot, A. de Lesquen, J. P. Merlo, and L. Van Rossum, Phys. Lett. 40B, 281 (1972).
[21]P. Johnson, K. E. Lassila, P. Koehler, R. Miller, and A. Yokosawa, Phys. Rev. Lett. 30, 242 (1973).
[22]R. L. Cool, G. Giacomelli, T. F. Kycia, B. A. Leontić, K. K. Li, A. Lundby, J. Teiger, and C. Wilken, Phys. Rev. D 1, 1887 (1970); R. J. Abrams, R. L. Cool, G. Giacomelli, T. F. Kycia, B. A. Leontić, K. K. Li, and D. N. Michael, *ibid.* 1, 1917 (1970).
[23]W. Galbraith, E. W. Jenkins, T. F. Kycia, B. A. Leontić, R. H. Phillips, and A. L. Read, Phys. Rev. 138, B913 (1965).
[24]S. P. Denisov, S. V. Donskov, Yu. P. Gorin, A. I. Petrukhin, Yu. D. Prokoshkin, and D. A. Stoyanova, Nucl. Phys. B65, 1 (1973).
[25]M. Lusignoli, M. Restignoli, G. A. Snow, and G. Violini, Nuovo Cimento 49A, 705 (1967).
[26]The data of Ref. 11 were excluded from this fit. This experiment (see Ref. 11) did not resolve the sharp forward peak in the $K_L^0 p \to K_S^0 p$ differential cross section, and thus substantially underestimated the cross section at $t = 0$.
[27]The uncertainties in $\Delta\sigma_{K^\pm n}^{tot}$ calculated as described were in fact larger than the uncertainties plus possible systematic errors quoted by Denisov *et al.* (see Ref. 24).
[28]R. Messner, R. Morse, U. Nauenberg, D. Hitlin, J. Liu, R. Piccioni, M. Schwartz, S. Wojcicki, and D. Dorfan, Phys. Rev. Lett. 30, 876 (1973).
[29]V. N. Bolotov, M. I. Devishev, V. V. Isakov, D. B. Kakauridze, V. A. Kachanov, V. M. Kutjin, Yu. D. Prokoshkin, E. A. Razuvaev, and V. K. Semenov, Serpukhov report, 1972 (unpublished).
[30]J. E. Nelson *et al.*, LBL Report No. LBL-1027, 1972 (unpublished); A. S. Carroll *et al.*, Phys. Rev. 177, 2047 (1969); M. A. Wahlig and I. Mannelli, *ibid.* 168, 1515 (1968); P. Sonderegger *et al.*, Phys. Lett. 20, 75 (1966); A. V. Stirling *et al.*, Phys. Rev. Lett. 14, 763 (1965); I. Mannelli *et al.*, *ibid.* 14, 408 (1965).
[31]G. Höhler and R. Strauss, Karlsruhe report, 1971 (unpublished).
[32]G. Höhler, J. Baacke, H. Schlaile, and P. Sonderegger, Phys. Lett. 20, 79 (1966).
[33]A. A. Hirata *et al.*, Nucl. Phys. B30, 157 (1971); M. Aguilar-Benitez, R. L. Eisner, and J. B. Kinson, Phys. Rev. D 4, 2583 (1971); I. Butterworth *et al.*, Phys. Rev. Lett. 15, 734 (1965); C. G. Wohl, UCRL-Report No. 16288, 1965 (unpublished); Y. Goldschmidt-Clermont *et al.*, Phys. Lett. 27B, 602 (1968); L. Moscoso *et al.*, *ibid.* 32B, 513 (1970); P. Astbury *et al.*, Phys. Lett. 23, 396 (1966); D. Cline, J. Penn, and D. D. Reeder, Nucl. Phys. B22, 247 (1970); A. Firestone *et al.*, Phys. Rev. Lett. 25, 958 (1970); G. C. Mason and C. G. Wohl, Oxford University report, 1973 (unpublished); R. Blokzijl *et al.*, Nucl. Phys. B51, 535 (1973); R. J. Miller *et al.*, Rutherford Report No. RPP/H/102, 1972 (unpublished). E. H. Willen *et al.*, BNL Report No. BNL 16681, 1972 (unpublished); V. N. Bolotov *et al.*, Serpukhov Report No. IHEP 73-53, 1973 (unpublished).
[34]M. Davier and H. Harari, Phys. Lett. 35B, 239 (1971).
[35]M. Ross, F. S. Henyey, and G. L. Kane, Nucl. Phys. B23, 269 (1970).
[36]R. J. Yamartino, Ph.D. thesis, Stanford University, 1973 (unpublished); A. C. Irving, A. D. Martin, and

V. Barger, CERN Report No. REF. TH 1585-CERN, 1972 (unpublished); J. A. J. Matthews, in π-π *Scattering 1973*, proceedings of the international conference on π-π scattering and associated topics, Tallahassee, 1973, edited by P. K. Williams and V. Hagopian (A.I.P., New York, 1973).

[37]Comparisons of the differential cross sections for $t<0$ from the helicity-flip-dominated reactions $\pi^- p \to \pi^0 n$, $\pi^- p \to \eta^0 n$ and KN charge exchange are in good agreement; see, for example, R. D. Matthews, Nucl. Phys. B11, 339 (1969).

[38]H. Harari, Ann. Phys. (N.Y.) 63, 432 (1971); Phys. Rev. Lett. 26, 1400 (1971).

[39]J. S. Loos and J. A. J. Matthews, Phys. Rev. D 6, 2463 (1972).

[40]W. Beusch *et al.*, Nucl. Phys. B19, 546 (1970); M. Pepin *et al.*, Phys. Lett. 26B, 35 (1967); D. J. Crennell *et al.*, Phys. Rev. D 6, 1220 (1972); O. I. Dahl *et al.*, Phys. Rev. 163, 1430 (1967).

[41]T. T. Wu and C. N. Yang, Phys. Rev. 137, B708 (1965); H. D. I. Abarbanel, S. D. Drell, and F. J. Gilman, Phys. Rev. Lett. 20, 280 (1968); S. M. Berman and M. Jacob, *ibid.* 25, 1683 (1970); G. Cocconi, Nuovo Cimento 57A, 837 (1968); S. M. Berman, J. D. Bjorken, and J. B. Kogut, Phys. Rev. D 4, 3388 (1971); J. F. Gunion, S. J. Brodsky, and R. Blankenbecler, Phys. Lett. 39B, 649 (1972).